Electromagnetic and gravitational outputs from binary neutron star coalescence

Carlos Palenzuela[1], Luis Lehner[2], Marcelo Ponce[3], Steven L. Liebling[4],
Matthew Anderson[5], David Neilsen[6], and Patrick Motl[7]
[1]Canadian Institute for Theoretical Astrophysics, Toronto, Ontario M5S 3H8, Canada,
[2]Perimeter Institute for Theoretical Physics,Waterloo, Ontario N2L 2Y5, Canada
[3]Department of Physics, University of Guelph, Guelph, Ontario N1G 2W1, Canada,
[4]Department of Physics, Long Island University, New York 11548, USA
[5] Pervasive Technology Institute, Indiana University, Bloomington, IN 47405, USA
[6]Department of Physics and Astronomy, Brigham Young University, Provo, Utah 84602, USA,
[7]Department of Science, Mathematics and Informatics, Indiana University Kokomo, Kokomo, IN 46904, USA,
(Dated:)

The late stage of an inspiraling neutron star binary gives rise to strong gravitational wave emission due to its highly dynamic, strong gravity. Moreover, interactions between the stellar magnetospheres can produce considerable electromagnetic radiation. We study this scenario using fully general relativistic, resistive magneto-hydrodynamics simulations. We show that these interactions extract kinetic energy from the system, dissipate heat, and power radiative Poynting flux, as well as develop current sheets. Our results indicate that this power can: (i) outshine pulsars in binaries, (ii) display a distinctive angular- and time-dependent pattern, and (iii) radiate within large opening angles. These properties suggest that some binary neutron star mergers are ideal candidates for multimessenger astronomy.

PACS numbers:

Introduction: Binary systems involving neutron stars are among the most likely sources of detectable gravitational waves (GW) for detectors such as Advanced LIGO/VIRGO. Among other insights these waves will provide fundamentally new clues about the population of these systems, constrain the equation of state of matter at nuclear densities, and provide sensitive tests of general relativity (e.g. [1]). Additionally, binary neutron stars (BNS) are thought to be progenitors of short gamma ray bursts (sGRB) [2–5] based on energetic, timescale and population considerations. These sGRBs are extremely energetic, beamed, extra-galactic events that last for less than a couple seconds; the origin of which has yet to be unambiguously determined.

Models associating BNS with sGRBs involve, at their core, the interaction of a black hole surrounded by a sufficiently massive disk, a situation that naturally arises after the collapse of the hypermassive neutron star resulting from a binary merger. The interaction of the central compact object with the accretion disk can power radiation with a hard spectrum and short time scale characteristic of sGRBs. Details about how the black hole or disk drives the radiation, such as via electromagnetic Poynting flux [6] or thermal energy deposition originated by neutrino-antineutrino annihilation [7], remain uncertain.

Correlating observations in both electromagnetic and GW bands has the potential to revolutionize our understanding of these systems. Examples of what can be gained from such correlations include: (i) timing information along with sky localization will test whether compact binaries are indeed engines of sGRBS, (ii) details from both bands will allow for breaking degeneracies in the physical parameters (e.g., masses, spins, orbital parameters, etc.) of the observed system, and (iii) determination of physical parameters will clarify the picture of the interaction of the binary with its environment (e.g. [8–11]). Additionally, low-latency GW analysis would allow for localizing a merging binary prior to the collision itself allowing suitable observatories to be in position to observe the main event (e.g. [12]).

While obvious candidates for such combined observations are sGRBs, it is important to note that not all sGRBs are observable in gamma rays, nor do all BNS mergers produce sGRBs, if any. An exciting possibility, provided by sky localization via gravitational waves, is the detection "orphan-GRB" afterglow signals [13, 14], induced by the interaction of the main burst with its environment. Additionally, EM signals preceding the merger might be detectable. Such EM precursors would be produced in a relatively cleaner environment, and so might provide crucial insight on physical parameters before the complicated, highly non-linear interactions expected during the merger epoch. One might also expect the system to radiate at an opening angle that decreases as the orbit tightens. Thus, precursors may be identifiable if GW analysis can provide adequate sky localization. Tantalizingly, some possible precursors have already been suggested [15].

Recently, magnetic interactions between the stars [16–21] and resonant crust cracking [22] have been proposed as possible precursor mechanisms. Here we focus on the former. The neutron stars making up the BNS are generally expected to maintain a roughly dipolar magnetic field and the stars are surrounded by a tenuous, mag-

netized plasma referred to as a *magnetosphere*. The interaction of the two stellar magnetospheres coupled with very dynamic gravity can produce a number of interactions and currents. The aim of this letter is to study the electromagnetic emission during the pre-merger stage of a BNS, to correlate it with the emitted gravitational waves, and to examine if the interaction of the magnetospheres can yield EM emissions strong enough to be detected.

Physical model: We focus on the last orbits of a binary of equal mass, magnetized, neutron stars in a quasi-circular orbit with initial separation $L = 45$ km, corresponding to an orbital frequency $\Omega_o = 1850$ rad/s. Each star has baryonic mass $M = 1.62\,M_\odot$ and stellar radius $R_* = 13.6$ km. The geometry and matter initial data for this system are obtained with the LORENE library [23], assuming a polytropic equation of state $P/c^2 = K\rho^\Gamma$ with $\Gamma = 2$ and $K = 123G^3M_\odot^2/c^6$, which approximates cold nuclear matter. During the evolution the stars are modeled with a magnetized perfect fluid with an ideal gas equation of state. Note that the dynamics and interactions of the electromagnetic (e.g. [20, 24, 25]) and gravitational (e.g. [26, 27]) fields are largely insensitive to the equation of state during the inspiral.

The stars have an initial, dipolar magnetic field $\mathbf{B}$ in each star's comoving frame described by a magnetic moment $\mu = B_*R_*^3$, with B_* the radial component at the pole of the star. To gain insight into the overall behavior of magnetized binaries we consider three related initial configurations of the magnetic moments, with directions specified with respect to the orbital angular momentum: aligned and equal magnetic moments (case U/U) with $\mu_1 = \mu_2 = \mu$, anti-aligned and equal magnetic moments (case U/D) with $\mu_1 = -\mu_2 = \mu$, and aligned magnetic moments with one-dominant moment (case U/u) with $\mu_1 = 100\,\mu_2 = \mu$. In our simulations we set $B_* = 1.5\times10^{11}$ G, a value on the high end of observations from binaries but still realistic. The last case (U/u) has parameters similar to those estimated in the double binary pulsar J0737-3039 [28].

We model this system within a fully consistent implementation that incorporates general relativity coupled to relativistic, resistive magnetohydrodynamics in full 3D. Details of our implementation are given in [24, 29–35]. Our numerical domain extends up to $L = 320$ km and contains five nested fixed mesh refinement (FMR) grids, each finer grid with twice the resolution of its parent grid. The highest resolution grid has $\Delta x = 300$ m and extends up to 58 km, covering both stars and the inner part of the magnetosphere. We have also compared coarser solutions of all the cases and the results are essentially unchanged.

Results: We place particular emphasis on electromagnetic effects as gravitational phenomena are reasonably well understood for this system (for a representative analysis of the late inspiral GW from this binary see e.g. [26]). The magnetic field has a negligible effect on the orbital dynamics of the system up to merger (e.g. [24, 25]), as its contribution to the total inertia is several orders of magnitude below that of the matter. The inspiral is well-described by a post-Newtonian chirp, independent of the magnetic field. Consequently, the merger progresses identically for all three cases, producing the same gravitational signal. The GW luminosity, to leading order, is $L_{\rm GW} \simeq 10^{55}\,(M/(2.9M_\odot))^{10/3}\,(\Omega/\Omega_{\rm ISCO})^{10/3}$ ergs/s (with M the total binary mass). We make use of a fiducial angular frequency $\Omega_{\rm ISCO} = 4758$ rad/s, chosen to be that of a particle at the inner-most, stable, circular orbit for a non-spinning black hole of mass $2.9M_\odot$ (this frequency is a good mark of the onset of the plunging behavior [26, 36]).

Because we focus on the late stage of coalescence, we choose initial data such that the stars orbit each other for approximately 2.5 orbits before merging. We follow the binary evolution through the merger stage, leaving the post-merger epoch analysis for future work. (For reference, we set $t = 0$ when the stars touch.)

In contrast to the orbital motion of the stars, the behavior of the electromagnetic field for all three cases depends sensitively on the orientation of the magnetic moment of the stars. At a basic level, the accelerated orbital motion of the stars induces only a small degree of winding on the magnetic fields; thus the magnetospheres essentially co-rotate with the stars while the magnetic field at the surface (and the magnetic moment) remains nearly constant until merger. As each star orbits within the magnetic field of the other, an electric field and currents are induced. Such interactions determine the topology of the resulting field and the net Poynting flux, as well as other relevant features. In regions where the magnetic field points in opposite directions, the plasma allows for reconnection of magnetic field lines, releasing significant energy. Reconnection can occur within *current sheets*, planar regions involving almost anti-parallel magnetic field lines supported by large current densities.

We display (a representative) late-time configuration of the magnetic field lines and current sheets for the various cases in Fig. 1. In the anti-aligned (U/D) and aligned (U/U) cases, a shear layer is induced at the midplane between the stars, separating two regions filled with magnetically dominated plasma moving in opposite directions. Interestingly, in the U/D case the poloidal component of the magnetic field points in opposite directions across the midplane, allowing for reconnections. The resulting magnetic field lines consequently connect both stars. As the stars orbit, these field lines are severely stretched, increasing their tension and developing a strong toroidal component. Near the leading edge of each stellar surface, these field lines undergo a twisting so extreme that they are bent almost completely backwards, allowing them to reconnect and release some of the orbital energy stored by the twisted magnetic fields.

Reconnection between the stars appears absent in the U/U case because the magnetic field points in the same

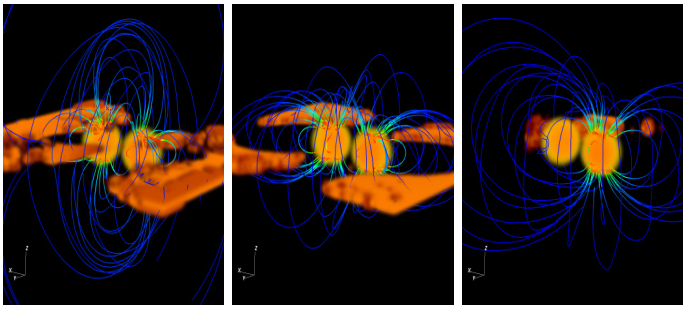

FIG. 1: Magnetic field configurations (field lines) and current sheets (orange regions) for –from left to right– the U/D, U/U and U/u cases at time $t = -1.7$ ms. In all panels, the magnetic field strength varies from 10^8 (blue) to 10^{11} (red) Gauss. The current sheet for the U/U case arises far outside the binary whereas that for the U/D case arises between the stars and spirals outward. A trailing dissipation tail is induced in the U/u case.

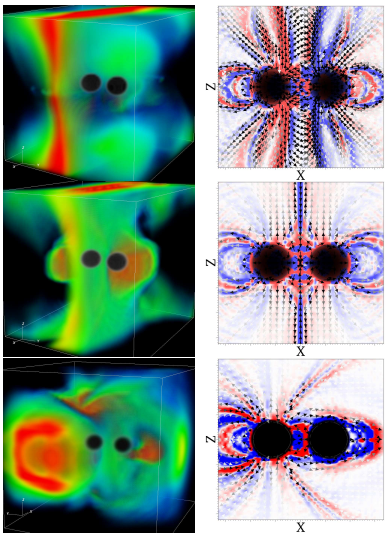

FIG. 2: Representative snapshots of the electromagnetic energy flux at $t = -2.9$ms [left column], and currents (arrows) and charge density (negative/positive shaded in red/blue) at $t = -0.5$ms [right column]; for the U/D, U/U and U/u cases (top/middle/bottom panels respectively). The U/D and U/U cases display currents extending significantly in both vertical directions, together with EM radiation mainly directed along the shear layer. In contrast, the currents are mostly localized in between the stars for the U/u case, with an energy flux concentrated near the equatorial plane. The color scales for the energy flux are arbitrary (with green to red spanning three orders of magnitude in scale, see Figure 3 for total luminosity vs time for each case). For comparison among the three cases we note that the U/D (U/U) case is three (two) orders of magnitude larger than the U/u case.

direction as one moves from one star to the other. Instead, far from the shear layer, the configuration resembles the dipole rotator solution of [37] that describes pulsar emission. This similarity is natural because the system has a net effective dipolar moment at leading order, though the symmetry of the binary system implies an (approximate) periodicity in the solution given by half the orbital period.

As the orbit proceeds, both the U/U and the U/D cases develop current sheets. In the U/D case, they begin between the stars on the orbital plane and propagate outwards in a spiral pattern. In the U/U case, the current sheet first arises at far distances. For rotating astrophysical systems, one defines the *light cylinder* as the radius at which the tangential linear velocity of a co-rotating magnetic field is equal to the speed of light. It is at the light cylinder for the U/U case that the current sheet first develops and continues inward, also with a spiral pattern, as the orbit tightens.

In case (U/u), the magnetic field of the first star eventually dominates that of the companion even near its surface. Thus, the field is largely described as an inspiraling dipole perturbed by the induction of the companion. An interesting effect arises as the magnetic field lines from the strongly magnetized star slide off the companion's surface and reconnect behind the star. This reconnection produces a dissipation tail as illustrated in Fig. 1. The extent of this tail gradually grows as the merger progresses, populating a localized current sheet behind the weakly magnetized star.

A qualitative understanding of the radiation from these three configurations, including the angular distribution, can be obtained from the Poynting flux shown in Fig. 2. Both the U/D and U/U cases radiate most strongly along the shear layer between the two stars and as a consequence their radiation is partially collimated. Indeed, the flux density in a polar cap (with opening angle of $\Theta_o < 30^o$) is larger than the average density by factors of 2.5× and 1.9×, accounting for 1/3 and 1/4 of the total power, respectively. In contrast, the U/u case radiates mainly on the equatorial plane and primarily in the direction of the strongly magnetized star with 2/3 of the total energy radiated between $60^o < \Theta_o < 90^o$.

A more quantitative measurement of the electromagnetic radiation of these systems is provided by integrating the Poynting flux over an encompassing sphere located at $R_{\rm ext} = 180$ km. Fig. 3 displays this Poynting luminosity as a function of time for the three configurations. It is interesting to note that the U/D case is significantly more radiative than the U/U case. In both cases, the "inner-engine" is powered by the magnetic field of each star and by their orbital motion, both of which share the same magnitude. The different luminosities therefore imply a more efficient tapping of orbital energy with anti-aligned magnetic moments (U/D) than when they are aligned (U/U), possibly due to the additional energy radiated by the release of magnetic tension in the U/D case through reconnections near the stars. Although the Poynting flux is generally not directly observable, this electromagnetic

energy can be transferred to kinetic energy of the plasma, which will radiate through different processes. A detailed understanding of these processes, even in the context of pulsars, is an active area of research. We use Poynting flux here as a first approximation to the energetics, and note that the mechanisms invoked for particle acceleration and emissions from pulsars (e.g. outer-gap, polar-cap, current sheets models) are applicable here as well.

The Poynting flux pattern and the current sheet structure for all cases rotate with a periodicity tied to the orbital motion. They thus trace the spacetime behavior and may help identify the system.

Analysis: To understand the behavior of the luminosities in Fig. 3, in particular their growth as the merger time is approached, we recall the *unipolar inductor* model of electromagnetic emission [38]. This model pictures a perfect conductor moving through an ambient magnetic field, inducing charge separation on its surface and driving currents. The translational kinetic energy from the moving conductor is extracted in the form of magnetohydrodynamic waves propagating along the magnetic field lines [39]. (We have studied magnetospheric interactions of binary black holes and found them well described by the unipolar behavior [30, 31, 40].) The expected luminosity from this model for a binary system composed of a magnetized primary star and an unmagnetized companion (for our masses and radii) is given approximately by [18–20]: $L_{\rm ind} \sim 10^{41}\,(B_*/10^{11}G)^2(\Omega/\Omega_{\rm ISCO})^{14/3}$ ergs/s.

The luminosities can be characterized in terms of powers of the orbital frequency of the binary as a function of time, $L \propto \Omega^p$ (assuming a constant surface magnetic field). For the U/u case, the early luminosity increases as $\Omega^{14/3}$, which is consistent with the unipolar inductor. At later times but still well before the stars touch, the luminosity increases much more rapidly, with $p \approx 12$. This slope is significantly steeper than the usual multipolar emissions. However, this behavior arises in the most dynamical stage with a rapidly changing multipolar structure, and such an analysis need not apply. We defer to future work a study focused on understanding this behavior.

The U/U and U/D cases differ from the expectation of the unipolar inductor. At early times, their luminosity increases with $p \simeq 1-2$ until the stars come into contact. For these two cases, the transition to rapid growth of luminosity (again with $p \approx 12$) occurs at later times than the U/u case. Interestingly, the agreement of the slopes for all the cases suggests that the dynamics near merger is dominated by the formation of the hypermassive neutron star, independent of the initial magnetic configuration.

Inspection of the induced currents indicates that all cases realize an effective circuit (see Fig. 2), albeit with different characteristics. In both the U/U and U/D cases, the circuit extends significantly in both vertical directions, which contrasts with the more localized currents

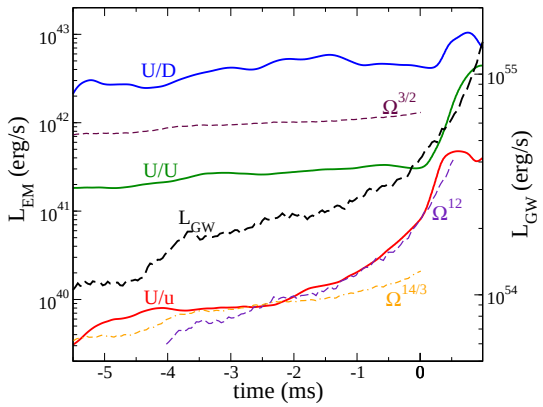

FIG. 3: Gravitational (right axis) and electromagnetic (left axis) luminosities for the three configurations vs time. Three curves illustrating $L \propto \Omega^p$ with $p = \{3/2, 14/3, 12\}$ are shown as guidance.

in the U/u case. The shape of the U/u currents roughly resemble those in the U/D case running from pole to pole and returning along a mostly equatorial path but are much smaller and restricted to the volume directly between the stars. In contrast, the U/U case preserves the symmetry between the stars and the current leaves the polar regions and returns along the midplane between the stars. As a last observation, we note that a significant amount of Joule heating ($J_i E^i$) is induced and deposited in the plasma between the stars. Relative to the Poynting flux, this heating is largest in the U/u case, being comparable to its electromagnetic energy radiated; for the U/D and U/U cases, on the other hand, the energy dissipated as heat is roughly 25–50% of their respective radiated energy. We thus stress that these systems display significant differences with respect to the predictions of the unipolar inductor model.

Discussion: We have shown that the interaction of the magnetospheres within a BNS can give rise to a rich structure that can power strong electromagnetic emissions ($\simeq 10^{40-43}(B/10^{11}{\rm G})^2$ erg/s) prior to merger. These luminosities are at, or higher than, that of the brightest pulsars and would bear characteristics tied to the orbital behavior. We have also identified features that can possibly lead to observable signals tied to the orbital behavior of the system. The time variability and large opening angle of possible emissions could help in their detection, especially if already localized in time and space by GW observation. (Binary neutron stars would spend roughly 30mins in band before merger, allowing for such detection with templates obtained via PostNewtonian approximations). Different emission mechanisms are expected near the current sheets, where strong cooling can give rise to gamma-rays [41, 42] produced via either synchrotron [41] or inverse Compton scattering [43] (see also discussion in [44]). Furthermore, accelerating

fields can arise naturally at gaps [45–48], energizing a population of particles that emit high energy curvature and synchrotron radiation. Understanding which of these mechanisms are the most relevant is yet unknown even in pulsar models so there is a large degree of uncertainty in this question. At a simple level however, a relativistically expanding electron-positron wind sourced by energy dissipation and magnetohydrodynamical waves in between the stars could create an X-ray signature [18] preceding or coincident with the merger. Thus, ISS-Lobster [49] with its high sensitivity and wide field of view would be very well suited for detecting the associated electromagnetic counterpart to a binary neutron star merger. Depending on how efficiently the Poynting flux is converted into radiation, these sources could be detectable over a large fraction of the range of advanced GW detectors.

Acknowledgments: It is a pleasure to thank A. Broderick, J. McKinney, A. Spitkovksy for discussions and Chris Thompson for discussions and comments on the manuscript. This work was supported by the NSF under grants PHY-0969827 (LIU), PHY-0969811 (BYU), NSERC through Discovery Grants (to LL), and NASA award NNX13AH01G. CP acknowledges support by the Jeffrey L. Bishop Fellowship. Research at Perimeter Institute is supported through Industry Canada and by the Province of Ontario through the Ministry of Research & Innovation. Computations were performed at XSEDE and Scinet.

[1] B. Sathyaprakash and B. Schutz, Living Rev.Rel. **12**, 2 (2009), 0903.0338.
[2] S. I. Blinnikov, I. D. Novikov, T. V. Perevodchikova, and A. G. Polnarev, Soviet Astronomy Letters **10**, 177 (1984).
[3] D. Eichler, M. Livio, T. Piran, and D. N. Schramm, Nature (London) **340**, 126 (1989).
[4] E. Nakar, Physics Reports **442**, 166 (2007), arXiv:astro-ph/0701748.
[5] E. Berger, New Aston. Rev. **55**, 1 (2011), 1005.1068.
[6] S. S. Komissarov, N. Vlahakis, A. Königl, and M. V. Barkov, Mon. Not. Roy. Astron. Soc. **394**, 1182 (2009), 0811.1467.
[7] M. A. Aloy, H.-T. Janka, and E. Müller, Astron. Astrophys. **436**, 273 (2005), arXiv:astro-ph/0408291.
[8] M. Branchesi, A. Klotz, and M. Laas-Bourez (LIGO Scientific Collaboration, Virgo Collaboration) (2011), 1110.3169.
[9] L. Z. Kelley, I. Mandel, and E. Ramirez-Ruiz (2012), 1209.3027.
[10] B. Sathyaprakash and B. F. Schutz, Living Reviews in Relativity **12** (2009), URL `http://www.livingreviews.org/lrr-2009-2`.
[11] J. S. Bloom, D. E. Holz, S. A. Hughes, K. Menou, A. Adams, et al. (2009), 0902.1527.
[12] J. Aasi et al. (LIGO Scientific Collaboration, Virgo Collaboration) (2013), 1304.0670.
[13] B. D. Metzger and E. Berger, Astrophys. J. **746**, 48 (2012), 1108.6056.
[14] T. Piran, E. Nakar, and S. Rosswog, Mon. Not. Roy. Astron. Soc. **430**, 2121 (2013), 1204.6242.
[15] E. Troja, S. Rosswog, and N. Gehrels, Astrophys.J. **723**, 1711 (2010), 1009.1385.
[16] V. M. Lipunov and I. E. Panchenko, Astron. Astrophys. **312**, 937 (1996), arXiv:astro-ph/9608155.
[17] M. Vietri, The Astrophysical Journal Letters **471**, L95 (1996).
[18] B. M. S. Hansen and M. Lyutikov, MNRAS **322**, 695 (2001), arXiv:astro-ph/0003218.
[19] A. L. Piro, Astrophys.J. **755**, 80 (2012), 1205.6482.
[20] D. Lai (2012), 1206.3723.
[21] M. Medvedev and A. Loeb (2012), 1212.0333.
[22] D. Tsang, J. S. Read, T. Hinderer, A. L. Piro, and R. Bondarescu, Physical Review Letters **108**, 011102 (2012), 1110.0467.
[23] LORENE. home page (2010), `http://www.lorene.obspm.fr/`.
[24] M. Anderson, E. W. Hirschmann, L. Lehner, S. L. Liebling, P. M. Motl, D. Neilsen, C. Palenzuela, and J. E. Tohline, Physical Review Letters **100**, 191101 (2008), 0801.4387.
[25] K. Ioka and K. Taniguchi, Astrophys.J. (2000), astro-ph/0001218.
[26] L. Baiotti, T. Damour, B. Giacomazzo, A. Nagar, and L. Rezzolla, Phys.Rev. **D84**, 024017 (2011), 1103.3874.
[27] J. S. Read, C. Markakis, M. Shibata, K. Uryu, J. D. Creighton, et al., Phys.Rev. **D79**, 124033 (2009), 0901.3258.
[28] M. Burgay, N. D'Amico, A. Possenti, R. N. Manchester, A. G. Lyne, B. C. Joshi, M. A. McLaughlin, M. Kramer, J. M. Sarkissian, F. Camilo, et al., Nature (London) **426**, 531 (2003), arXiv:astro-ph/0312071.
[29] L. Lehner, C. Palenzuela, S. L. Liebling, C. Thompson, and C. Hanna, Phys.Rev. **D86**, 104035 (2012), 1112.2622.
[30] C. Palenzuela, L. Lehner, and S. L. Liebling, Science **329**, 927 (2010), 1005.1067.
[31] D. Neilsen, L. Lehner, C. Palenzuela, E. W. Hirschmann, S. L. Liebling, et al., Proc.Nat.Acad.Sci. **108**, 12641 (2011), 1012.5661.
[32] C. Palenzuela, L. Lehner, O. Reula, and L. Rezzolla, Mon.Not.Roy.Astron.Soc. **394**, 1727 (2009), 0810.1838.
[33] C. Palenzuela, M. Anderson, L. Lehner, S. L. Liebling, and D. Neilsen, Phys. Rev. Lett. **103**, 081101 (2009), 0905.1121.
[34] S. Chawla, M. Anderson, M. Besselman, L. Lehner, S. L. Liebling, P. M. Motl, and D. Neilsen, Phys. Rev. Lett. **105**, 111101 (2010).
[35] C. Palenzuela, Mon. Not. Roy. Astron. Soc. **431**, 1853 (2013), 1212.0130.
[36] A. Buonanno, L. E. Kidder, and L. Lehner, Phys. Rev. **D77**, 026004 (2008), 0709.3839.
[37] A. Spitkovsky, Astrophys.J. **648**, L51 (2006), astro-ph/0603147.
[38] P. Goldreich and D. Lynden-Bell, Astrophys. J. **156**, 59 (1969).
[39] S. D. Drell, H. M. Foley, and M. A. Ruderman, Physical Review Letters **14**, 171 (1965).
[40] C. Palenzuela, T. Garrett, L. Lehner, and S. L. Liebling, Phys. Rev. **D82**, 044045 (2010), 1007.1198.
[41] D. A. Uzdensky and A. Spitkovsky (2012), 1210.3346.
[42] D. A. Uzdensky, Space Science Reviews **160**, 45 (2011),

1101.2472.
[43] M. Lyutikov, ArXiv e-prints (2012), 1208.5329.
[44] J. Arons, A&AS **120**, C49 (1996).
[45] R. W. Romani and I.-A. Yadigaroglu, Astrophys. J. **438**, 314 (1995), arXiv:astro-ph/9401045.
[46] K. S. Cheng, M. Ruderman, and L. Zhang, Astrophys. Journal **537**, 964 (2000).
[47] A. G. Muslimov and A. K. Harding, Astrophys.J. **588**, 430 (2003), astro-ph/0301023.
[48] A. G. Muslimov and A. K. Harding, Astrophys.J. **606**, 1143 (2004), astro-ph/0402462.
[49] J. Camp, S. D. Barthelmy, L. Blackburn, K. Carpenter, N. Gehrels, et al. (2013), 1304.3705.